Acta Crystallographica Section B
**Structural Science**
ISSN 0108-7681

# Equilibrium langbeinite-related phosphates $Cs_{1+x}Ln_xZr_{2-x}(PO_4)_3$ (Ln = Sm–Lu) in the melted systems $Cs_2O$–$P_2O_5$–$LnF_3$–$ZrF_4$

**Ivan V. Ogorodnyk,[a]* Vyacheslav N. Baumer,[b] Igor V. Zatovsky,[a] Nikolay S. Slobodyanik,[a] Oleg V. Shishkin[b] and Konstantin V. Domasevitch[a]**

[a]Department of Inorganic Chemistry, Taras Shevchenko National University, 64 Volodymyrska str., Kyiv 01033, Ukraine, and [b]STC 'Institute for Single Crystals', NAS of Ukraine, 60 Lenin Avenue, Kharkiv 61001, Ukraine

Correspondence e-mail: ogorod@bigmir.net

Received 23 May 2007
Accepted 9 October 2007

Nine novel phosphates, based upon a combination of caesium, zirconium and lanthanide ions, were obtained from fluoride-containing fluxes using high-temperature crystallization. The structures of $Cs_{1.80}Eu_{0.80}Zr_{1.20}(PO_4)_3$ (CsEuZrP), $Cs_{1.79}Gd_{0.79}Zr_{1.21}(PO_4)_3$ (CsGdZrP), $Cs_{1.87}Tb_{0.87}Zr_{1.13}(PO_4)_3$ (CsTbZrP), $Cs_{1.67}Dy_{0.67}Zr_{1.33}(PO_4)_3$ (CsDyZrP), $Cs_{1.75}Ho_{0.75}Zr_{1.25}(PO_4)_3$ (CsHoZrP), $Cs_{1.78}Er_{0.78}Zr_{1.22}(PO_4)_3$ (CsErZrP), $Cs_{1.70}Tm_{0.70}Zr_{1.30}(PO_4)_3$ (CsTmZrP), $Cs_{1.52}Yb_{0.52}Zr_{1.48}(PO_4)_3$ (CsYbZrP) and $Cs_{1.63}Lu_{0.63}Zr_{1.37}(PO_4)_3$ (CsLuZrP) were solved using single-crystal X-ray diffraction. All compounds are isostructural to the mineral langbeinite (cubic system, space group $P2_13$). Their framework structures originate from the cross-linking of metal octahedra [$MO_6$] ($M$ = Zr, $Ln$) by phosphate tetrahedra. $Cs^+$ cations are located in the closed cavities of the framework and preferentially occupy one of the two available sites. The principles of crystallization of the equilibrium langbeinite-related phosphates in the fluxes of the system $Cs_2O$–$P_2O_5$–$LnF_3$–$ZrF_4$ (Ln = La–Nd, Sm–Lu) are discussed based on their crystal structures.

## 1. Introduction

A wide variety of langbeinite-related compounds are known. Besides the mineral langbeinite $K_2Mg_2(SO_4)_3$ (cubic system, space group $P2_13$; Zemann & Zemann, 1957), which is found in nature, a number of synthetic compounds belonging to this large family are known, including sulfates, phosphates and vanadates. The preparation of phosphates with the langbeinite structure is associated with the synthesis of compounds related to $NaZr_2(PO_4)_3$ (NZP, which crystallizes in the space group $R3c$; Hagman & Kierkegaard, 1968) during which langbeinites are often formed. The latter compounds can be explained by the relations between the two structural types. The compounds have similar framework features and involve common building units, but with different spatial packing. Generally, the structure consists of small network cations in an octahedral oxygen environment connected to each other *via* the tetrahedral anion units. The rigid frameworks form large closed cavities in the case of langbeinite or infinite open tunnels in the case of NASICON ('$Na^+$-ion superionic conductor'), both of which incorporate alkali metal monocations, and this difference leads to some subtle differences within these structural types. Thus, unlike common NASICON-related compounds containing lithium cations [$LiZr_2(PO_4)_3$; Petit *et al.*, 1986], lithium langbeinites are unknown. In addition, a number of alkali-ion-free frameworks isotypic with NZP [$Fe_{0.5}Nb_{1.5}(PO_4)_3$; Trubach, Orlova *et al.*, 2004] have been obtained, while langbeinite-related compounds with empty cavities are unknown.

Complex phosphates of langbeinite structure are represented by a diversity of compounds, prepared by employing various network cations and with the utilization of different synthetic techniques, such as the methods of flux growth as well as solid state and hydrothermal reactions. A number of large mono- or polyvalent cations have been tested for their ability to serve as cavity cations. For sodium, $Na_2MTi(PO_4)_3$ ($M$ = Fe, Cr) were obtained and characterized by Isasi & Daidouh (2000), while the group of potassium-containing langbeinites is the largest: $KTi_2(PO_4)_3$ (Masse *et al.*, 1972), $K_2Ti_2(PO_4)_3$ (Leclaire *et al.*, 1989), $K_{1+x}Ti_{2-y}Al_y(PO_4)_3$ (Slobodyanik *et al.*, 1991), $K_2CrTi(PO_4)_3$ (Boudjada & Perret, 1977; Norberg, 2002), $A_2MTi(PO_4)_3$, $A$ = K, Rb, Tl; $M$ = Cr, Fe (Perret & Boudjada, 1979), $K_2VTi(PO_4)_3$ (Rangan & Gopalakrishnan, 1994), $K_2MTi(PO_4)_3$, $M$ = Er, Yb, Y (Norberg, 2002), $K_2M_{0.5}Ti_{1.5}(PO_4)_3$, $M$ = Mn, Co, Ni (Ogorodnyk, Zatovsky, Slobodyanik *et al.*, 2006; Ogorodnyk *et al.*, 2007), $K_2MZr(PO_4)_3$, $M$ = Y, Gd (Wulff *et al.*, 1992), $K_2FeZr(PO_4)_3$ (Orlova *et al.*, 2003), $K_2LnZr(PO_4)_3$, Ln = Ce–Lu (Trubach *et al.*, 2004*b*), $K_2BiHf(PO_4)_3$ (Losilla *et al.*, 1998), $K_{11}V_{15}(PO_4)_{18}O$ (Benmoussa *et al.*, 1992) and $K_{11}Fe_{15}(PO_4)_{18}O$ (Lajmi *et al.*, 2003). Rubidium-containing langbeinites are much more scarce: $Rb_2FeZr(PO_4)_3$ (Trubach *et al.*, 2004*a*), $Rb_2YbTi(PO_4)_3$ and $Rb_2Yb_{0.32}Ti_{1.68}(PO_4)_3$ (Gustafsson *et al.*, 2005), $Rb_2Mg_{0.5}Zr_{1.5}(PO_4)_3$ (Orlova *et al.*, 2005), $Rb_2YTi(PO_4)_3$ (Gustafsson *et al.*, 2006). $Cs_2Mg_{0.5}Zr_{1.5}(PO_4)_3$ (Orlova *et al.*, 2005), however, is the only example with caesium cations in the cavities. Phosphates with the langbeinite structure containing only barium or only lead cations [$Ba_{1.5}V_2(PO_4)_3$; Droß & Glaum, 2004; $Pb_{1.5}V_2(PO_4)_3$; Shpanchenko *et al.*, 2005] are also relatively rare. Another interesting group of phosphate langbeinites are compounds containing multiple cations: $KBaFe_2(PO_4)_3$ (Battle *et al.*, 1986), $KBaCr_2(PO_4)_3$ (Battle *et al.*, 1988) and $(NH_4)(H_3O)$-$Ti_2(PO_4)_3$ (Fu *et al.*, 2005).

Herein, we report the synthesis and structural characterization of a new subgroup of phosphates with the langbeinite structure that is based on a combination of zirconium and lanthanide cations with caesium cations incorporated in the cavities. Their general composition is as follows: $Cs_{1+x}Ln_xZr_{2-x}(PO_4)_3$, where Ln = Sm–Lu. Principles of the crystallization of equilibrium langbeinite-related phosphates in the fluxes of the system $Cs_2O$–$P_2O_5$–$LnF_3$–$ZrF_4$ (Ln = La–Nd, Sm–Lu) will be discussed on the basis of the crystal structure.

## 2. Experimental

### 2.1. Synthetic procedure

A new technique for crystal growth from fluxes was utilized in the preparation of the titled langbeinites beginning with fluoride precursors containing zirconium ($ZrF_4$) and lanthanide ($LnF_3$, where Ln = La–Nd, Sm–Lu). The solubility of $ZrO_2$ in phosphate fluxes is very low and the main phases which are often obtained in such cases are NZP-related $M^IZr_2(PO_4)_3$ (Sljukic *et al.*, 1969; Hagman & Kierkegaard, 1968; Gobechiya *et al.*, 2004) or $M^I_2Zr(PO_4)_2$ (Doerffel & Liebertz, 1991). The well shaped crystals of NZP grow during the dissolving of zirconium dioxide even when the temperature is above 1500 K. Therefore, it is difficult to synthesize compounds other than NZP or $M^I_2Zr(PO_4)_2$ zirconium phosphates using flux crystallization of pure phosphate systems by the usual techniques. In contrast, $ZrF_4$ melts when injected into the phosphate flux and yields a true solution. As the latter process is accompanied by the thermohydrolysis of the fluoride, it is necessary to perform the high-temperature synthesis as quickly as possible. This is the reason why the second precursor is also a metal fluoride, as $LnF_3$ has a higher reactivity than the corresponding oxide.

Calculated amounts of $ZrF_4$ and $LnF_3$ were added to the homogenous melt of $CsPO_3$ with constant stirring using a platinum stirrer. The flux was then cooled to crystallize the compound. This technique was examined in the synthesis of $K_4CeZr(PO_4)_4$ (Ogorodnyk, Zatovsky, Baumer *et al.*, 2006).

$CsPO_3$ was prepared in two steps. The first step was the neutralization of a water solution of CsOH by a calculated amount of $H_3PO_4$. The $CsH_2PO_4$ solution was then boiled to evaporate the remaining water; after evaporation it was cooled to 273 K. In the next step crystals of $CsH_2PO_4$ were separated from the mother liquor and decomposed at 900 K for 6 h to obtain $CsPO_3$. The completeness of the $CsH_2PO_4$ decomposition was examined using powder XRD and FTIR spectroscopy.

To investigate the interactions in the system $CsPO_3$–$ZrF_4$–$LnF_3$ melts, the following procedures were then performed. $CsPO_3$ (8 g, 37.75 mmol) was placed into a platinum crucible and heated to 1273 K to obtain the flux. The temperature was then decreased to 1223 K and a ground mixture of $ZrF_4$ (0.567 g, 3.39 mmol) and $LnF_3$ (Ln = La–Lu; 0.655–0.788 g, 3.39 mmol) was added to the flux with stirring. The melts were cooled to 833 K at a rate of 25 K $h^{-1}$. At this temperature the liquid glass containing the crystals was poured from the crucible onto a copper sheet to freeze the crystallization processes. The glass was washed with hot deionized water to separate the crystals. The total yield of the crystalline products was *ca* 1–1.5 g.

Phase analyses for all obtained samples were performed using powder XRD. The experiment was carried out using a Siemens D500 automated diffractometer (Cu $K\alpha$ radiation, $\lambda$ = 1.54184 Å; curved graphite monochromator on the counter arm; step size 0.02°; range 5–90°; scanning rate 10 s per point). Single crystals possessing the tetrahedral langbeinite habit were manually separated from the reaction product mixtures. Their chemical composition was verified by energy-dispersive spectroscopy using a Link Isis analyzer mounted on a Philips XL 30 FEG scanning electron microscope. The established atomic ratios were close to those calculated during the crystal structure refinement. The single-crystal X-ray diffraction experiments were performed on the same crystals used for elemental analysis.

### 2.2. Data collection and data refinement

All data were collected with an Oxford Diffraction XCalibur 3 CCD diffractometer [Mo $K\alpha$ radiation, $\lambda$ = 0.71073 Å; graphite monochromator; $\varphi$ and $\omega$ scans; temperature 293 (2) K]. An empirical multi-scan absorption correction of the obtained data was applied (Blessing, 1995). Symmetry-equivalent reflections were averaged while keeping the Friedel pairs separated. The structures were solved by direct methods using *SHELXS*97 (Sheldrick, 1997*a*) for the location of the primary sites for Cs, Ln and P atoms, while the positions of the four O atoms were found from Fourier synthesis performed during full-matrix refinement. It was assumed that the Zr atoms occupy the same sites as the Ln atoms. Their coordinates and ADPs (atomic displacement parameters) were constrained and their occupancies were refined using the linear combination of free variable restraints (SUMP) for both positions (site occupancy = 1.00) of the octahedrally coordinated metal. At the same time the occupancies of the Cs atoms were freely refined in the initial phase of the refinement. As a result, the compositions obtained were close to those reported. For a better agreement between the charge of the cationic and anionic components, the total cationic charge was restrained (charge = 9.00). An extinction correction was applied for all the compounds investigated, but as its value was found to be negligible (compared with its standard error) it was removed from the final cycles of the refinement in several of the structures.

Experimental parameters are listed in Table 1,[1] and the occupancies of Cs, Zr and Ln positions, and selected geometric parameters are gathered in Table 2.

## 3. Results and discussion

### 3.1. Structure description

Complex compounds, which belong to the langbeinite family (sulfates, phosphates, vanadates *etc.*) are well described in the literature. Several alternative descriptions of their framework have been proposed. One of them describes the structure on the basis of $[M_2X_3O_{18}]$ units, which are formed from two octahedra interconnected using three phosphate bridges. The second approach considers the larger $[M_5X_6O_{39}]$ units that provide a possibility for the description of the cavities (Norberg, 2002). The term packed ⟨111⟩ rods was used by O'Keeffe & Andersson (1977) to describe the packing symmetry in these structures.

Combining these representations of the crystal structure results in the following description. The simplest building elements are isolated octahedra and tetrahedra. A pair of the nearest metal octahedra is interlinked *via* three phosphate tetrahedra forming the $[M_2P_3O_{18}]$ blocks. In the reported compounds, they stack along the [111] direction at a distance of *ca* 10.8 Å. Using $[M_2X_3O_{18}]$ as the starting building units, we replaced two octahedra by a cylinder and omitted all the phosphate bridges. The dimensions of the cylinder are close to the dimensions of the $M_2P_3O_{18}$ group where three phosphate tetrahedra are omitted. This is illustrated in the legend of Fig. 1. The cylinders with definite dimensions allow for the observation of the packing of the structural elements. O'Keeffe *et al.* (2001) describe this packing as Γ packing. The cylinders retain the general symmetry of the packing, but also make visible the cavities in the framework (Fig. 1*b*). Eight

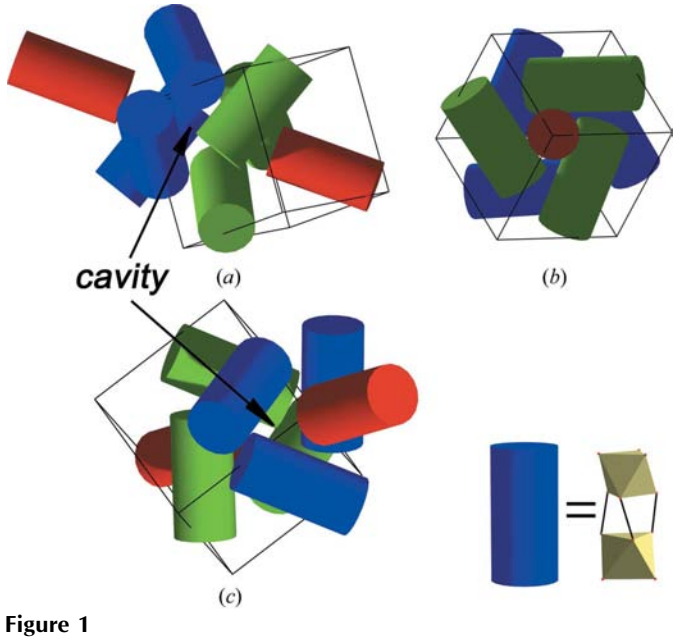


**Figure 1**
Model of packing cylinders in (*a*) the langbeinite structure, (*b*) view along the [111] direction and (*c*) the best view of the cavity. The three groups of cylinders are differently colored for the best visualization of the cavity. Two red cylinders are top and bottom; three green (one layer) and three blue (another layer) are the sides of the cavity.

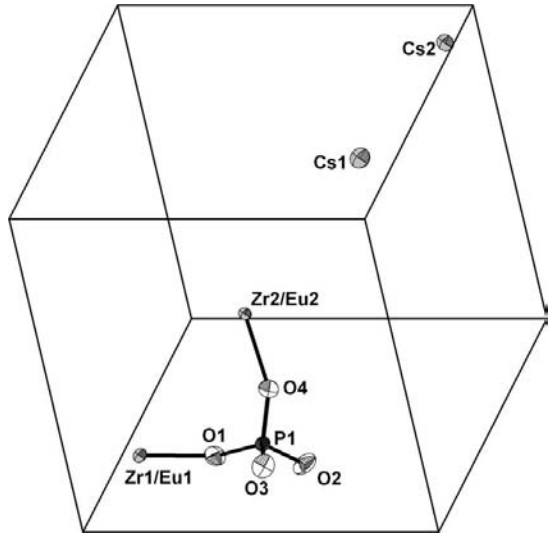


**Figure 2**
View of $Cs_{1.80}Eu_{0.80}Zr_{1.20}(PO_4)_3$ (CsEuZrP) (70% probability displacement ellipsoids).

[1] Supplementary data for this paper are available from the IUCr electronic archives (Reference: SX5073). Services for accessing these data are described at the back of the journal.

**Table 1**
Experimental details.

| | CsEuZrP | CsGdZrP | CsTbZrP | CsDyZrP | CsHoZrP |
|---|---|---|---|---|---|
| Crystal data | | | | | |
| Chemical formula | $Cs_{1.805}Eu_{0.805}Zr_{1.195}(PO_4)_3$ | $Cs_{1.793}Gd_{0.793}Zr_{1.207}(PO_4)_3$ | $Cs_{1.87}Tb_{0.87}Zr_{1.13}(PO_4)_3$ | $Cs_{1.67}Dy_{0.67}Zr_{1.33}(PO_4)_3$ | $Cs_{1.745}Ho_{0.745}Zr_{1.255}(PO_4)_3$ |
| $M_r$ | 756.34 | 757.86 | 775.00 | 736.46 | 754.40 |
| Cell setting, space group | Cubic, $P2_13$ | Cubic, $P2_13$ | Cubic, $P2_13$ | Cubic, $P2_13$ | Cubic, $P2_13$ |
| Temperature (K) | 293 (2) | 293 (2) | 293 (2) | 293 (2) | 293 (2) |
| $a$ (Å) | 10.49690 (10) | 10.4752 (5) | 10.4920 (12) | 10.42900 (10) | 10.43720 (10) |
| $V$ (Å$^3$) | 1156.60 (2) | 1149.44 (10) | 1155.0 (2) | 1134.30 (2) | 1136.98 (2) |
| $Z$ | 4 | 4 | 4 | 4 | 4 |
| $D_x$ (Mg m$^{-3}$) | 4.344 | 4.379 | 4.457 | 4.313 | 4.407 |
| Radiation type | Mo $K\alpha$ | Mo $K\alpha$ | Mo $K\alpha$ | Mo $K\alpha$ | Mo $K\alpha$ |
| $\mu$ (mm$^{-1}$) | 11.48 | 11.70 | 12.59 | 11.34 | 12.29 |
| Crystal form, color | Tetrahedron, colorless | Tetrahedron, colorless | Tetrahedron, colorless | Tetrahedron, colorless | Tetrahedron, pale yellow |
| Crystal size (mm) | 0.07 × 0.06 × 0.04 | 0.08 × 0.07 × 0.05 | 0.1 × 0.08 × 0.07 | 0.14 × 0.1 × 0.08 | 0.12 × 0.1 × 0.09 |
| Data collection | | | | | |
| Diffractometer | XCalibur-3 | XCalibur-3 | XCalibur-3 | XCalibur-3 | XCalibur-3 |
| Data collection method | $\varphi$ and $\omega$ scans | $\varphi$ and $\omega$ scans | $\varphi$ and $\omega$ scans | $\varphi$ and $\omega$ scans | $\varphi$ and $\omega$ scans |
| Absorption correction | Multi-scan (based on symmetry-related measurements) | Multi-scan (based on symmetry-related measurements) | Multi-scan (based on symmetry-related measurements) | Multi-scan (based on symmetry-related measurements) | Multi-scan (based on symmetry-related measurements) |
| $T_{min}$ | 0.415 | 0.463 | 0.294 | 0.317 | 0.319 |
| $T_{max}$ | 0.541 | 0.600 | 0.432 | 0.433 | 0.403 |
| No. of measured, independent and observed reflections | 7245, 1137, 1094 | 13 339, 1127, 1125 | 8906, 942, 923 | 5951, 1108, 1068 | 4066, 1108, 1043 |
| Criterion for observed reflections | $I > 2\sigma(I)$ | $I > 2\sigma(I)$ | $I > 2\sigma(I)$ | $I > 2\sigma(I)$ | $I > 2\sigma(I)$ |
| $R_{int}$ | 0.031 | 0.033 | 0.037 | 0.054 | 0.032 |
| $\theta_{max}$ (°) | 30.0 | 30.0 | 28.2 | 29.9 | 29.9 |
| Refinement | | | | | |
| Refinement on | $F^2$ | $F^2$ | $F^2$ | $F^2$ | $F^2$ |
| $R[F^2 > 2\sigma(F^2)]$, $wR(F^2)$, $S$ | 0.017, 0.029, 1.17 | 0.012, 0.029, 1.37 | 0.017, 0.048, 1.25 | 0.031, 0.070, 1.16 | 0.024, 0.043, 1.21 |
| No. of reflections | 1137 | 1127 | 942 | 1108 | 1108 |
| No. of parameters | 65 | 65 | 64 | 64 | 65 |
| Weighting scheme | $w = 1/[\sigma^2(F_o^2) + (0.0095P)^2 + 1.2265P]$, where $P = (F_o^2 + 2F_c^2)/3$ | $w = 1/[\sigma^2(F_o^2) + (0.009P)^2 + 1.6865P]$, where $P = (F_o^2 + 2F_c^2)/3$ | $w = 1/[\sigma^2(F_o^2) + (0.0277P)^2 + 1.4032P]$, where $P = (F_o^2 + 2F_c^2)/3$ | $w = 1/[\sigma^2(F_o^2) + (0.0366P)^2 + 4.5336P]$, where $P = (F_o^2 + 2F_c^2)/3$ | $w = 1/[\sigma^2(F_o^2) + (0.0106P)^2 + 3.0354P]$, where $P = (F_o^2 + 2F_c^2)/3$ |
| $(\Delta/\sigma)_{max}$ | 0.001 | 0.001 | 0.003 | 0.003 | 0.001 |
| $\Delta\rho_{max}$, $\Delta\rho_{min}$ (e Å$^{-3}$) | 0.47, −0.62 | 0.56, −0.45 | 0.87, −0.90 | 0.90, −0.98 | 0.75, −0.68 |
| Extinction method | *SHELXL* | *SHELXL* | None | None | *SHELXL* |
| Extinction coefficient | 0.00046 (9) | 0.00044 (9) | – | – | 0.00062 (15) |
| Absolute structure | Flack (1983) | Flack (1983) | Flack (1983) | Flack (1983) | Flack (1983) |
| Flack parameter | 0.01 (2) | 0.012 (19) | 0.02 (3) | −0.01 (4) | 0.00 (3) |
| EDX analysis, found atomic ratio | | | | | |
| Cs:Zr:Ln:P | 1.85:1.21:0.82:3.00 | 1.81:1.21:0.78:3.00 | 1.91:1.15:0.88:3.00 | 1.71:1.35:0.71:3.00 | 1.76:1.27:0.77:3.00 |

| | CsErZrP | CsTmZrP | CsYbZrP | CsLuZrP |
|---|---|---|---|---|
| Crystal data | | | | |
| Chemical formula | $Cs_{1.775}Er_{0.775}Zr_{1.225}(PO_4)_3$ | $Cs_{1.70}Tm_{0.70}Zr_{1.30}(PO_4)_3$ | $Cs_{1.515}Yb_{0.515}Zr_{1.485}(PO_4)_3$ | $Cs_{1.625}Lu_{0.625}Zr_{1.375}(PO_4)_3$ |
| $M_r$ | 762.12 | 748.46 | 710.85 | 735.89 |
| Cell setting, space group | Cubic, $P2_13$ | Cubic, $P2_13$ | Cubic, $P2_13$ | Cubic, $P2_13$ |
| Temperature (K) | 293 (2) | 293 (2) | 293 (2) | 293 (2) |
| $a$ (Å) | 10.4142 (2) | 10.39820 (10) | 10.36160 (10) | 10.38651 (17) |
| $V$ (Å$^3$) | 1129.48 (4) | 1124.28 (2) | 1112.45 (2) | 1120.49 (3) |
| $Z$ | 4 | 4 | 4 | 4 |
| $D_x$ (Mg m$^{-3}$) | 4.482 | 4.422 | 4.244 | 4.362 |
| Radiation type | Mo $K\alpha$ | Mo $K\alpha$ | Mo $K\alpha$ | Mo $K\alpha$ |
| $\mu$ (mm$^{-1}$) | 12.97 | 12.64 | 11.07 | 12.46 |
| Crystal form, color | Tetrahedron, rose | Tetrahedron, grey | Tetrahedron, colorless | Tetrahedron, colorless |
| Crystal size (mm) | 0.08 × 0.07 × 0.05 | 0.05 × 0.05 × 0.04 | 0.07 × 0.06 × 0.04 | 0.08 × 0.07 × 0.06 |

**Table 1 (continued)**

| | CsErZrP | CsTmZrP | CsYbZrP | CsLuZrP |
|---|---|---|---|---|
| Data collection | | | | |
| Diffractometer | XCalibur-3 | XCalibur-3 | XCalibur-3 | XCalibur-3 |
| Data collection method | $\varphi$ and $\omega$ scans | $\varphi$ and $\omega$ scans | $\varphi$ and $\omega$ scans | $\varphi$ and $\omega$ scans |
| Absorption correction | Multi-scan (based on symmetry-related measurements) | Multi-scan (based on symmetry-related measurements) | Multi-scan (based on symmetry-related measurements) | Multi-scan (based on symmetry-related measurements) |
| $T_{min}$ | 0.429 | 0.560 | 0.515 | 0.337 |
| $T_{max}$ | 0.569 | 0.622 | 0.669 | 0.423 |
| No. of measured, independent and observed reflections | 5508, 1108, 1065 | 4789, 1093, 1048 | 4844, 1096, 981 | 3891, 1104, 1053 |
| Criterion for observed reflections | $I > 2\sigma(I)$ | $I > 2\sigma(I)$ | $I > 2\sigma(I)$ | $I > 2\sigma(I)$ |
| $R_{int}$ | 0.038 | 0.033 | 0.036 | 0.026 |
| $\theta_{max}$ (°) | 30.0 | 30 | 30.0 | 30.0 |
| Refinement | | | | |
| Refinement on | $F^2$ | $F^2$ | $F^2$ | $F^2$ |
| $R[F^2 > 2\sigma(F^2)]$, $wR(F^2)$, $S$ | 0.026, 0.042, 1.29 | 0.025, 0.040, 1.20 | 0.020, 0.035, 0.96 | 0.016, 0.033, 1.09 |
| No. of reflections | 1108 | 1093 | 1096 | 1104 |
| No. of parameters | 64 | 64 | 64 | 65 |
| Weighting scheme | $w = 1/[\sigma^2(F_o^2) + (0.0000P)^2 + 5.3017P]$, where $P = (F_o^2 + 2F_c^2)/3$ | $w = 1/[\sigma^2(F_o^2) + (0.006P)^2 + 4.3663P]$, where $P = (F_o^2 + 2F_c^2)/3$ | $w = 1/[\sigma^2(F_o^2) + (0.014P)^2]$, where $P = (F_o^2 + 2F_c^2)/3$ | $w = 1/[\sigma^2(F_o^2) + (0.0158P)^2]$, where $P = (F_o^2 + 2F_c^2)/3$ |
| $(\Delta/\sigma)_{max}$ | 0.006 | 0.002 | 0.001 | 0.001 |
| $\Delta\rho_{max}$, $\Delta\rho_{min}$ (e Å$^{-3}$) | 0.88, −0.96 | 0.74, −0.81 | 0.75, −0.70 | 0.49, −0.48 |
| Extinction method | None | None | None | *SHELXL* |
| Extinction coefficient | – | – | – | 0.00084 (15) |
| Absolute structure | Flack (1983) | Flack (1983) | Flack (1983) | Flack (1983) |
| Flack parameter | 0.05 (3) | −0.01 (2) | −0.02 (2) | 0.014 (16) |
| EDX analysis, found atomic ratio | | | | |
| Cs:Zr:Ln:P | 1.79:1.24:0.78:3.00 | 1.71:1.32:0.69:3.00 | 1.53:1.50:0.52:3.00 | 1.64: 1.39: 0.62: 3.00 |

Computer programs used: *CrysAlis CCD* (Oxford Diffraction Ltd, 2005*a*), *CrysAlis RED* (Oxford Diffraction Ltd, 2005*b*), *SHELXS*97 (Sheldrick, 1997*a*), *SHELXL*97 (Sheldrick, 1997*b*), *DIAMOND* (Brandenburg, 2006), *WinGX* (Farrugia, 1999).

such blocks form a cavity and large cations occupy these sites (Figs. 1*a* and *c*).

*M*1 and *M*2 sites are occupied by the octahedrally coordinated Zr and Ln (Ln = Eu–Lu) atoms (Fig. 2). Lanthanide atoms are mainly located in the *M*2 position, while zirconium atoms are preferentially located at *M*1. The occupancies of the *M*2 positions for the lanthanide atoms are close to $\frac{1}{2}$ and the remaining quantities of lanthanide occupy the *M*1 site (less than one third). In both the $[M1O_6]$ and the $[M2O_6]$ octahedra the metal atoms appear slightly displaced from the polyhedron center (Table 2). At the same time the $[M2O_6]$ octahedra are compresed along the threefold axis, as indicated by the values of the O3—*M*2—O3 (I) and O4—*M*2—O4 (II) angle sum ($\Sigma_{I+II} > 180°$, with the exception of the Yb compound). It should be noted that the degree of compression decreases in the CsEuZrP–CsLuZrP row. The {O1—O1—O1} and {O2—O2—O2} faces of the $[M1O_6]$ octahedron, and the {O3—O3—O3} and {O4—O4—O4} faces of the $[M2O_6]$ octahedron are coparallel (Fig. 3). The distances between these pairs of planes can be used for the characterization of the metal-ion octahedral coordination. These values show the same behaviour with the degree of compression decreasing as the value of the ionic radii (Shannon, 1976) of the elements decreases (Fig. 4). A wide spread in the octahedral thickness values for $[M1O_6]$ can be explained by the dispersion of the occupancies of the lanthanide ions in the *M*1 position. Bond-valence sums (BVSs) for the metals (Table 3) in their octahedral oxygen environments were calculated using the parameters from Brese & O'Keeffe (1991). The values for zirconium are lower than 4 and for the lanthanide they are much higher than 3. Such behaviour of the BVS values is related to the fact that both types of atoms are located in the same positions, while their bonding parameters differ significantly. In these structures, calculated during the structure refinement, values of *M*—O bonds could be presented as the linear sum of Zr—O and Ln—O bonds, taking into account the fraction of each bond which corresponds (is equal) to the occupancies of Zr and Ln. Two cases are possible for this pair of atoms. The first can be observed, for example, in $K_4CeZr(PO_4)_4$ (Ogorodnyk, Zatovsky, Baumer *et al.*, 2006), where Ce and Zr atoms are located in the same position. Two different oxygen environments for Ce and Zr were proposed on the basis of BVS calculations and the structural investigations. The calculated values of the BVS values were found to be 4.00 for $Zr^{IV}$ (six-coordinated, octahedron) and 4.09 for $Ce^{IV}$ (eight-coordinated, dodecahedron). The other case can be observed when

**Table 2**
Occupancies of Cs, Zr, Ln positions and selected geometric parameters (Å, °).

| | CsEuZrP | CsGdZrP | CsTbZrP | CsDyZrP | CsHoZrP |
|---|---|---|---|---|---|
| Cs1 | 0.994 (2) | 1.010 (2) | 1.016 (3) | 0.991 (3) | 0.995 (3) |
| Cs2 | 0.8121 (19) | 0.7830 (18) | 0.855 (3) | 0.676 (3) | 0.751 (3) |
| Zr1 | 0.703 (3) | 0.703 (2) | 0.657 (3) | 0.783 (3) | 0.7392 (9) |
| Zr2 | 0.4909 (9) | 0.5040 (9) | 0.4722 (9) | 0.5499 (9) | 0.515 (3) |
| Ln1 | 0.297 (3) | 0.296 (2) | 0.343 (3) | 0.217 (3) | 0.2607 (9) |
| Ln2 | 0.5090 (9) | 0.4959 (9) | 0.5278 (9) | 0.4500 (9) | 0.485 (3) |
| Shift from the octahedron center† | | | | | |
| *M*1 | 0.039 (3) | 0.031 (2) | 0.031 (3) | 0.020 (5) | 0.023 (4) |
| *M*2 | 0.033 (3) | 0.032 (3) | 0.035 (3) | 0.024 (4) | 0.026 (3) |
| *M*1—O1 | 2.120 (3) | 2.114 (3) | 2.119 (4) | 2.089 (5) | 2.106 (4) |
| *M*1—O2$^{i}$ | 2.139 (3) | 2.128 (2) | 2.137 (4) | 2.107 (5) | 2.114 (4) |
| *M*2—O3$^{ii}$ | 2.169 (3) | 2.160 (2) | 2.156 (4) | 2.142 (5) | 2.143 (4) |
| *M*2—O4 | 2.196 (3) | 2.182 (2) | 2.186 (4) | 2.157 (5) | 2.159 (4) |
| O3$^{ii}$—M2—O3$^{iii}$ (I) | 91.83 (11) | 91.65 (10) | 91.90 (15) | 91.29 (19) | 91.43 (16) |
| O4—M2—O4$^{iv}$ (II) | 89.52 (10) | 89.49 (9) | 89.55 (14) | 89.50 (18) | 89.53 (15) |
| Σ(I + II) | 181.35 | 181.14 | 181.45 | 180.79 | 180.96 |
| P1—O1 | 1.540 (3) | 1.541 (2) | 1.543 (4) | 1.549 (5) | 1.540 (4) |
| P1—O2 | 1.533 (3) | 1.534 (3) | 1.534 (4) | 1.538 (5) | 1.535 (4) |
| P1—O3 | 1.526 (3) | 1.528 (3) | 1.540 (4) | 1.527 (5) | 1.529 (4) |
| P1—O4 | 1.531 (3) | 1.536 (2) | 1.538 (4) | 1.540 (5) | 1.541 (4) |
| Cs1—O range | 3.127 (3)–3.338 (3) | 3.128 (2)–3.337 (3) | 3.125 (4)–3.333 (4) | 3.129 (5)–3.321 (6) | 3.117 (4)–3.320 (5) |
| Cs2—O range | 3.071 (3)–3.324 (3) | 3.064 (3)–3.327 (3) | 3.064 (4)–3.338 (4) | 3.052 (5)–3.320 (5) | 3.053 (4)–3.319 (4) |
| ⟨Cs1—O⟩ | 3.253 (3) | 3.250 (3) | 3.251 (4) | 3.238 (6) | 3.237 (5) |
| ⟨Cs2—O⟩ | 3.221 (3) | 3.214 (3) | 3.220 (4) | 3.199 (5) | 3.202 (4) |

| | CsErZrP | CsTmZrP | CsYbZrP | CsLuZrP |
|---|---|---|---|---|
| Cs1 | 1.004 (3) | 1.003 (3) | 0.988 (2) | 0.9853 (19) |
| Cs2 | 0.771 (3) | 0.701 (2) | 0.5275 (18) | 0.6412 (15) |
| Zr1 | 0.7088 (9) | 0.741 (3) | 0.829 (2) | 0.778 (2) |
| Zr2 | 0.517 (3) | 0.5559 (9) | 0.6562 (9) | 0.5962 (9) |
| Ln1 | 0.2911 (9) | 0.259 (3) | 0.171 (2) | 0.222 (2) |
| Ln2 | 0.483 (3) | 0.4441 (9) | 0.3436 (9) | 0.4037 (9) |
| Shift from the octahedron center† | | | | |
| *M*1 | 0.025 (4) | 0.014 (3) | 0.012 (3) | 0.009 (3) |
| *M*2 | 0.026 (3) | 0.029 (3) | 0.024 (3) | 0.024 (3) |
| *M*1—O1 | 2.102 (4) | 2.098 (4) | 2.093 (3) | 2.090 (3) |
| *M*1—O2$^{i}$ | 2.111 (4) | 2.101 (4) | 2.081 (3) | 2.094 (3) |
| *M*2—O3$^{ii}$ | 2.130 (4) | 2.116 (4) | 2.107 (3) | 2.112 (3) |
| *M*2—O4 | 2.151 (4) | 2.146 (4) | 2.126 (3) | 2.137 (3) |
| O3$^{ii}$—*M*2—O3$^{iii}$ (I) | 91.32 (16) | 91.16 (15) | 90.80 (12) | 90.89 (10) |
| O4—*M*2—O4$^{iv}$ (II) | 89.49 (15) | 89.27 (13) | 89.00 (11) | 89.30 (10) |
| Σ(I + II) | 180.81 | 180.43 | 179.8 | 180.19 |
| P1—O1 | 1.538 (4) | 1.539 (4) | 1.534 (3) | 1.549 (3) |
| P1—O2 | 1.534 (4) | 1.534 (4) | 1.539 (3) | 1.539 (3) |
| P1—O3 | 1.531 (4) | 1.538 (4) | 1.534 (3) | 1.535 (3) |
| P1—O4 | 1.540 (4) | 1.536 (4) | 1.535 (3) | 1.536 (3) |
| Cs1—O range | 3.108 (4)–3.306 (4) | 3.114 (4)–3.303 (4) | 3.127 (3)–3.287 (3) | 3.111 (3)–3.293 (3) |
| Cs2—O range | 3.048 (4)–3.320 (4) | 3.045 (4)–3.324 (4) | 3.036 (3)–3.322 (3) | 3.045 (3)–3.329 (3) |
| ⟨Cs1–O⟩ | 3.228 (4) | 3.226 (4) | 3.217 (3) | 3.218 (3) |
| ⟨Cs2—O⟩ | 3.194 (4) | 3.190 (4) | 3.181 (3) | 3.188 (3) |

Symmetry codes: (i) $x-\frac{1}{2},\frac{1}{2}-y,-z$; (ii) $1-x,\frac{1}{2}+y,\frac{1}{2}-z$; (iii) $\frac{1}{2}+y,\frac{1}{2}-z,1-x$; (iv) $y,z,x$. † The octahedron center was calculated as the geometrical mean of the distance between parallel sides and was placed on a threefold axis.

the environment of two different ions situated in the same position is the same. In this case the BVS values differ appreciably from the chemical valences. In $Rb_2YbTi(PO_4)_3$ (Gustafsson *et al.*, 2005) the BVS was found to be 2.62 for $Ti1^{IV}$, 3.36 for $Ti2^{IV}$, 3.93 for Yb1 and 5.00 for Yb2. Similar deviations of the BVS values from chemical valences can also

**Table 3**
Bond-valence sums for CsLnZrP.

| | CsEuZrP | CsGdZrP | CsTbZrP | CsDyZrP | CsHoZrP |
|---|---|---|---|---|---|
| Cs1(nine-coordinate) | 1.06[a]; 0.94[c] | 0.98[a]; 0.87[c] | 0.97[a]; 0.87[c] | 1.00[a]; 0.89[c] | 1.01[a]; 0.90[c] |
| Cs2(12-coordinate) | 1.56[a]; 1.37[c] | 1.45[a]; 1.28[c] | 1.43[a]; 1.27[c] | 1.51[a]; 1.33[c] | 1.50[a]; 1.32[c] |
| Zr1 | 3.57[b] | 3.65[b] | 3.58[b] | 3.88[b] | 3.76[b] |
| Ln1 | 5.19[b] | 5.16[b] | 4.85[b] | 5.08[b] | 4.74[b] |
| ***M*1** | **3.99** | **4.02** | **3.97** | **4.12** | **3.99** |
| Zr2 | 3.09[b] | 3.19[b] | 3.19[b] | 3.38[b] | 3.37[b] |
| Ln2 | 4.50[b] | 4.51[b] | 4.32[b] | 4.42[b] | 4.25[b] |
| ***M*2** | **3.74** | **3.78** | **3.74** | **3.81** | **3.77** |
| P1 | 5.03[a] | 5.00[a] | 4.94[a] | 4.95[a] | 4.98[a] |
| $\sum$ **(for formula unit)** | **24.87** | **24.68** | **24.50** | **24.56** | **24.59** |

| | CsErZrP | CsTmZrP | CsYbZrP | CsLuZrP |
|---|---|---|---|---|
| Cs1(nine-coordinate) | 1.03[a]; 0.92[c] | 1.04[a]; 0.92[c] | 1.05[a]; 0.93[c] | 1.06[a]; 0.94[c] |
| Cs2(12-coordinate) | 1.53[a]; 1.35[c] | 1.55[a]; 1.36[c] | 1.59[a]; 1.39[c] | 1.56[a]; 1.37[c] |
| Zr1 | 3.80[b] | 3.87[b] | 4.00[b] | 3.95[b] |
| Ln1 | 4.62[b] | 4.59[b] | 4.56[b] | 4.33[b] |
| ***M*1** | **4.02** | **4.04** | **4.09** | **4.03** |
| Zr2 | 3.46[b] | 3.55[b] | 3.69[b] | 3.62[b] |
| Ln2 | 4.22[b] | 4.21[b] | 4.21[b] | 3.96[b] |
| ***M*2** | **3.81** | **3.83** | **3.86** | **3.75** |
| P1 | 4.98[a] | 4.97[a] | 4.99[a] | 4.93[a] |
| $\sum$ **(for formula unit)** | **24.73** | **24.66** | **24.57** | **24.37** |

Bond-valence parameters from references: (*a*) Brown & Altermatt (1985); (*b*) Brese & O'Keeffe (1991); (*c*) Adams (2001).

be observed for the present structures. Dispersion of the corresponding BVS values in these compounds can be explained by the dispersion of the occupancies of Zr and Ln in the corresponding positions. To compare the environments of the two metal sites, *M*1 and *M*2, we modified the equation

$$s = \exp((R_0 - R)/B)$$

using values of $R_0$ calculated from the equation

$$R_0 = R_0(\mathrm{Zr}) \times \mathrm{Oc}(\mathrm{Zr}) + R_0(\mathrm{Ln}) \times \mathrm{Oc}(\mathrm{Ln}),$$

where $R_0$(Zr) and $R_0$(Ln) are bond-valence parameters and Oc(Zr) and Oc(Ln) are the crystallographic occupancies. The mean-calculated effective BVS value for the *M*1 position is $4.03 \pm 0.08$ and for the *M*2 position is $3.79 \pm 0.07$ in the compounds reported.

The geometry of the tetrahedral [$PO_4$] group is similar in the nine structures. P—O bond lengths are characteristic of the orthophosphate group and O—P—O angles are close to tetrahedral. The BVS for the P atom approaches 5.

Cs1 is nine-coordinated, while Cs2 is 12-coordinated. A recently proposed description assumes that the cations in the cavity are surrounded by [$MO_6$] octahedral units (Gustafsson *et al.*, 2005). According to this point of view the atom in the Cs1 position is linked to six neighboring octahedra and adopts an octahedral arrangement, while the atom in the Cs2 position is coordinated by only four octahedra in a tetrahedral arrangement. Cs—O distances which describe the oxygen environment of the Cs atoms are spread over the range [3.036 (3)–3.338 (3) Å] for all the compounds investigated. Generally, the Cs—O interatomic distances become shorter in the Eu–Lu row. For the 12-coordinated Cs2 atom the Cs—O bond length range is wider [3.036 (3)–3.338 (4) Å] than for the nine-coordinated Cs1 atom [3.108 (4)–3.338 (3) Å]. Some general points should

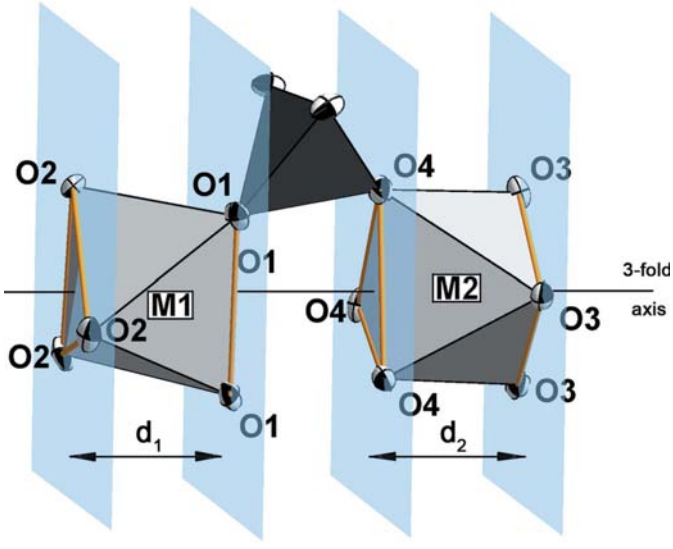


**Figure 3**
Parallel faces of the [$M1O_6$] and [$M2O_6$] octahedra.

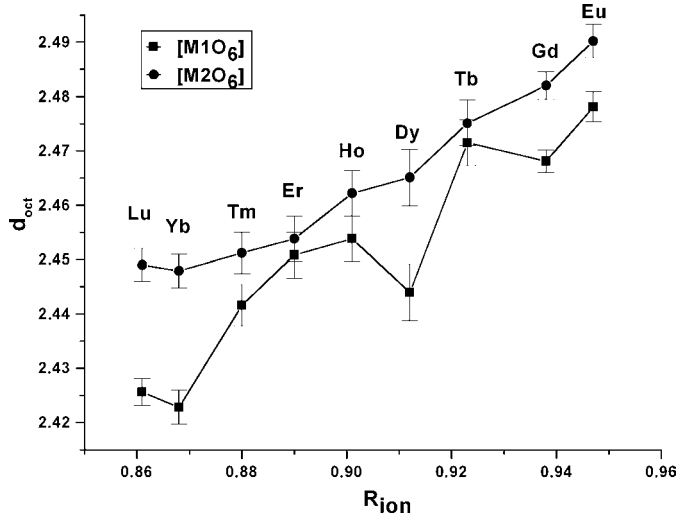


**Figure 4**
Graphical dependence of the dimensions of the octahedra (distances between parallel sides of the octahedra) along the [111] direction from the ionic radii of the corresponding lanthanide.

be noted about the occupancy values of the metal positions. The Cs1 site is fully (or close to fully) occupied, while the 12-coordinated Cs2 site is only partially filled. We have calculated the BVS values to compare the coordination environment of the Cs atoms (Table 3) and have examined the bonding parameters from (*a*) Brown & Altermatt (1985) and (*c*) Adams (2001). For all the reported structures, the corresponding values of the BVS are similar, but they differ significantly for the two Cs atoms. The values calculated on the basis of parameters from (*a*) are significantly lower than those taken from (*c*). Comparing the BVS for Rb in the previous work (Gustafsson *et al.*, 2005) and the BVS for Cs in the current work it should be noted that the values of BVS for Rb are equal to 0.82 and 1.06 for the nine- and 12-coordinated Rb atoms, respectively [$Rb_2YbTi(PO_4)_3$ at 293 K], while the value for the nine-coordinated Cs1 atom is close to 1 and is significantly higher (1.27–1.59) for the 12-coordinated Cs2 atom. Thus, the general trend of BVS values of the alkaline metal atoms is retained, but the values for caesium are unreasonable. This may be attributed to significant differences in the ionic radii of the Rb and Cs cations populating the same crystal cavities in $Rb_2YbTi(PO_4)_3$ [the values of the Rb—O bonds are in the range 2.966 (5)–3.306 (6) Å for the 12-coordinated atom and 2.990 (5)–3.305 (6) Å for the nine coordinated atom] and in the compounds investigated. Taking into account the BVS for the Cs atoms the nine-coordinated Cs1 position is more favourable for Cs insertion than the 12-coordinated Cs2 position, which confirms the experimental values of the distribution of Cs atoms over the two sites in the whole series of reported compounds.

The sum of the valences of the negatively charged O atoms is equal to −24 per formula unit. The sums of the calculated values of BVS for the positively charged phosphorus and metal atoms (employing effective BVS values for the *M*1 and *M*2 positions) is insignificantly higher, near +25. The high BVS values for the Cs atoms and decreasing Cs—O interatomic distances with decreasing ionic radii of the network cations mitigate against the crystallization of langbeinite-related phosphates containing Cs in the cavities and cations with radii less than that of Lu in the framework. On the other hand, the insertion of Cs cations could be facilitated by the expansion of the cavity size. A suitable cavity size could be supported by langbeinites containing octahedrally coordinated lanthanide elements with ionic radii larger than that of Sm. However, in our experiments we did not obtain langbeinite-related phosphates with the lanthanides Ln = La–Nd. This can be explained by the fact that langbeinite frameworks containing large lanthanides are unstable. Since the geometry of the [$PO_4$] group is rigid, as the dimensions of the [$MO_6$] increase the phosphate group becomes rather small for linking the large octahedra into the three-dimensional framework. The preparation of langbeinite-related compounds containing caesium and large lanthanides (Ln = La–Nd) should be possible if the phosphate group were to be completely or partially substituted by a larger building block, for example [$AsO_4$], [$MoO_4$] or [$WO_4$].

### 3.2. Interactions in the flux system $Cs_2O$–$P_2O_5$–$LnF_3$–$ZrF_4$ (Ln = La–Nd, Sm–Lu)

The chemical behaviour of the lanthanides are similar owing to their electron-shell configuration. The differences which are observed are related to their ionic radii and valence forms. We investigated the $Cs_2O$–$P_2O_5$–$LnF_3$–$ZrF_4$ (Ln = La–Nd, Sm–Lu) system over wide ranges of Cs:P molar ratios (1.0–1.4) and at different concentrations of the metal fluorides (4.5–13% mol. for each fluoride component). The synthetic conditions reported in §2 were selected to be those which optimize the crystal growth of the langbeinite-related phases. The general composition of the equilibrium langbeinite-like compounds obtained can be described as $Cs_{1+x}Ln_xZr_{2-x}(PO_4)_3$, where Ln = Sm–Lu. When the concentration of the $ZrF_4$ is much higher than that of $LnF_3$, then NASICON-related phases were additionally obtained. Further, when the concentration of the lanthanide fluoride is higher, then the additional phases are monazite ($LnPO_4$, Ln = La–Gd) or $CsLnP_2O_7$ (Ln = Dy–Lu) or both (in the case where Ln = Tb). Needle-like $CsLnP_2O_7$ grows isostructurally to $CsYbP_2O_7$ (Jansen *et al.*, 1991). At higher Cs:P molar ratios the amount of $CsLnP_2O_7$ increases in the mixtures obtained. This observation could be explained by the depolymerization of the polyphosphate chains. The highest fraction of $CsLnP_2O_7$ was observed in the system containing ytterbium (the fraction is near 30%). The smaller amount of Yb in the corresponding langbeinite could possibly be explained by the precipitation of the less-soluble caesium ytterbium diphosphate $CsYbP_2O_7$ from the equilibrium melt. In the system where Ln = La–Nd, we could not obtain phosphates isostructural with langbeinite, and the only crystalline products were monazites $LnPO_4$. For the system containing Sm, the formation of langbeinite-shaped crystals was detected, but only in addition to the main product, the monazite $SmPO_4$. The fraction of samarium-containing langbeinite is less than 10% (molar). We could not perform the single-crystal X-ray diffraction experiment. All of the selected crystals were well shaped, but cloudy and Debye rings were observed in the diffraction images. It can be assumed that the samarium is the element with the largest ionic radius that can form langbeinites from the equilibrium fluxes and pair with caesium as the large monovalent cation bound in the cavities.

The authors acknowledge the ICDD for financial support (Grant #03-02).

## References

Adams, St. (2001). *Acta Cryst.* B**57**, 278–287.
Battle, P. D., Cheetham, A. K., Harrison, W. T. A. & Long, G. J. (1986). *J. Solid State Chem.* **62**, 16–25.
Battle, P. D., Gibb, T. C., Nixon, S. & Harrison, W. T. A. (1988). *J. Solid State Chem.* **75**, 21–29.
Benmoussa, A., Borel, M. M., Grandin, A., Leclaire, A. & Raveau, B. (1992). *J. Solid State Chem.* **97**, 314–318.
Blessing, R. H. (1995). *Acta Cryst.* A**51**, 33–38.
Boudjada, A. & Perret, R. (1977). *J. Appl. Cryst.* **10**, 129.

Brandenburg, K. (2006). *DIAMOND*, Version 3.1c. University of Bonn, Germany.
Brese, N. E. & O'Keeffe, M. (1991). *Acta Cryst.* B**47**, 192–197.
Brown, I. D. & Altermatt, D. (1985). *Acta Cryst.* B**41**, 244–247.
Doerffel, M. & Liebertz, J. (1991). *Z. Kristallogr.* **193**, 155–159.
Droß, T. & Glaum, R. (2004). *Acta Cryst.* E**60**, i58–i60.
Farrugia, L. J. (1999). *J. Appl. Cryst.* **32**, 837–838.
Flack, H. D. (1983). *Acta Cryst.* A**39**, 876–881.
Fu, Y.-L., Xu, Z.-W., Ren, J.-L. & Ng, S. W. (2005). *Acta Cryst.* E**61**, i158–i159.
Gobechiya, E. R., Kabalov, Yu. K., Pet'kov, V. I. & Sukhanov, M. V. (2004). *Crystallogr. Rep.* **49**, 741–746.
Gustafsson, J. C. M., Norberg, S. T. & Svensson, G. (2006). *Acta Cryst.* E**62**, i160–i162.
Gustafsson, J. C. M., Norberg, S. T., Svensson, G. & Albertsson, J. (2005). *Acta Cryst.* C**61**, i9–i13.
Hagman, L. O. & Kierkegaard, P. (1968). *Acta Chem. Scand.* **22**, 1822–1832.
Isasi, J. & Daidouh, A. (2000). *Solid State Ion.* **133**, 303–313.
Jansen, M., Wu, G. Q. & Koenigstein, K. (1991). *Z. Kristallogr.* **197**, 245–246.
Lajmi, B., Hidouri, M., Wattiaux, A., Fournés, L., Darriet, J. & Ben Amara, M. (2003). *J. Alloys Compd.* **361**, 77–83.
Leclaire, A., Benmoussa, A., Borel, M. M., Grandin, A. & Raveau, B. (1989). *J. Solid State Chem.* **78**, 227–231.
Losilla, E. R., Bruque, S., Aranda, M. A. G., Moreno-Real, L., Morin, E. & Quarton, M. (1998). *Solid State Ion.* **112**, 53–62.
Masse, R., Durif, A., Guitel, J. C. & Tordjman, I. (1972). *Bull. Soc. Fr. Mineral. Crystallogr.* **95**, 47–55.
Norberg, S. T. (2002). *Acta Cryst.* B**58**, 743–749.
O'Keeffe, M. & Andersson, S. (1977). *Acta Cryst.* A**33**, 914–923.
O'Keeffe, M., Plévert, J., Teshima, Y., Watanabe, Y. & Ogama, T. (2001). *Acta Cryst.* A**57**, 110–111.
Ogorodnyk, I. V., Zatovsky, I. V., Baumer, V. N., Slobodyanik, N. S. & Shishkin, O. V. (2006). *Acta Cryst.* C**62**, i100–i102.
Ogorodnyk, I. V., Zatovsky, I. V. & Slobodyanik, N. S. (2007). *Russ. J. Inorg. Chem.* **52**, 121–125.
Ogorodnyk, I. V., Zatovsky, I. V., Slobodyanik, N. S., Baumer, V. N. & Shishkin, O. V. (2006). *J. Solid State Chem.* **179**, 3461–3466.
Orlova, A. I., Orlova, V. A., Beskrovnyi, A. I., Trubach, I. G. & Kurazhkovskaya, V. S. (2005). *Crystallogr. Rep.* **50**, 759–765.
Orlova, A. I., Trubach, I. G., Kurazhkovskaya, V. S., Pertierra, P., Salvadó, M. A., García-Granda, S., Khainakov, S. A. & García, J. R. (2003). *J. Solid State Chem.* **173**, 314–318.
Oxford Diffraction Ltd (2005*a*). *CrysAlis CCD*, Version 1.171.28p4beta, Release 11–11-2005 CrysAlis171.NET. Oxford Diffraction Ltd, Abingdon, Oxfordshire.
Oxford Diffraction Ltd (2005*b*). *CrysAlis RED*, Version 1.171.28p4beta, Release 11–11-2005 CrysAlis171.NET. Oxford Diffraction Ltd, Abingdon, Oxfordshire.
Perret, R. & Boudjada, A. (1979). *C. R. Acad. Sci. Ser. C*, **288**, 525–527.
Petit, D., Colomban, Ph., Collin, G. & Boilot, J. P. (1986). *Mater. Res. Bull.* **21**, 365–371.
Rangan, K. K. & Gopalakrishnan, J. (1994). *J. Solid State Chem.* **109**, 116–121.
Shannon, R. D. (1976). *Acta Cryst.* A**32**, 751–767.
Sheldrick, G. M. (1997*a*). *SHELXS*97. University of Göttingen, Germany.
Sheldrick, G. M. (1997*b*). *SHELXL*97. University of Göttingen, Germany.
Shpanchenko, R. V., Lapshina, O. A., Antipov, E. V., Hadermann, J., Kaul, E. E. & Geibel, C. (2005). *Mater. Res. Bull.* **40**, 1569–1576.
Sljukic, M., Matkovic, B., Prodic, B. & Anderson, D. (1969). *Z. Kristallogr.* **130**, 148–161.
Slobodyanik, N. S., Stus, N. V., Nagornyi, P. G. & Kapshuk, A. A. (1991). *Russ. J. Inorg. Chem.* **36**, 1554–1556.
Trubach, I. G., Beskrovnyi, A. I., Orlova, A. I., Orlova, V. A. & Kurazhkovskaya, V. S. (2004*a*). *Crystallogr. Rep.* **49**, 895–898.
Trubach, I. G., Beskrovnyi, A. I., Orlova, A. I., Orlova, V. A. & Kurazhkovskaya, V. S. (2004*b*). *Crystallogr. Rep.* **49**, 614–618.
Trubach, I. G., Orlova, A. I., Beskrovnyi, A. I., Koryttseva, A. K., Zharinova, M. V., Kurazhkovskaya, V. S. & Lipatova, E. V. (2004). *Crystallogr. Rep.* **49**, 396–400.
Wulff, H., Guth, U. & Loescher, B. (1992). *Powder Diffr.* **7**, 103–106.
Zemann, A. & Zemann, J. (1957). *Acta Cryst.* **10**, 409–413.